Two-photon processes at Belle

H. Nakazawa[1)]
National Central University, Chung-Li

Abstract We review recent measurements of pure neutral final state production in the two-photon processes, $\gamma\gamma \to \pi^0\pi^0$ and $\eta\pi^0$ at the Belle experiment. In the lower invariant mass region, properties of light scalar mesons are measured by partial wave analysis. In the higher energy region the total and differential cross section are compared with QCD models.

Key words two-photon, cross section, resonance

PACS 12.38.Bx, 12.38.Qk, 13.25.Jx

1 Introduction

Two-photon production of exclusive hadronic final states provides useful information about resonances and pertubative and nonperturbative QCD. From theoretical viewpoint, two-photon process is attractive because of the absence of strong interactions in the initial state and the possibility of calculating $\gamma\gamma \to q\bar{q}$ amplitudes. In addition, the quantum numbers of the final state are restricted to states of charge conjugation $C = +1$ with $J = 1$ forbidden. This feature enables us to do complementary measurement to e^+e^- annihilation process where mesons with $C = -1$ and $J = 1$ are produced exclusively.

We have measured charged pion pair [1–3], charged kaon pair [1, 4], neutral kaon pair [5], proton antiproton pair [6] and D-meson pair [7] production in two-photon collisions. The statistics of these measurements is 2 to 3 orders of magnitude highter than in the pre-B-factory measurements, opening a new era in studies of two-photon physics.

In this report, we summarize measurements of neutral final state production, $\gamma\gamma \to \pi^0\pi^0$ and $\eta\pi^0$. We use the data samples of 95 fb^{-1} [8] and 223 fb^{-1} [9] for $\gamma\gamma \to \pi^0\pi^0$ and of 223 pb^{-1} for $\gamma\gamma \to \eta\pi^0$ [10] collected with the Belle detector [11] at the energy-asymmetric e^+e^- KEKB collider [12].

2 Derivation of differential cross sections

The differential cross section for pair production in two-photon collision, $\gamma\gamma \to h\bar{h'}$ is obtained by

$$\frac{d\sigma}{d|\cos\theta^*|} = \frac{\Delta Y - \Delta B}{\Delta W \Delta|\cos\theta^*|\,\epsilon\, L_{\gamma\gamma}\int Ldt}, \qquad (1)$$

where ΔY and ΔB are the numbers of signal and background events, respectively, found in a bin width of the two-photon invariant mass ΔW and $\Delta|\cos\theta^*|$ with θ^* a scattering angle of h with respect to the gamma beam in two-photon center of mass system, $\epsilon(W, |\cos\theta^*|)$, $L_{\gamma\gamma}(W)$ and $\int Ldt$ are the efficiency, luminosity function and integrated luminosity, respectively.

3 Event selection

To reconstruct π^0 and η, photons are detected and measured in an electromagnetic calorimeter (ECL) which is an array of 8736 CsI(Tl) crystals pointing toward the interaction point. Signals from ECL are also used to issue an energy trigger which requires total energy deposit greater than 1.15 GeV, or a four or more cluster trigger each of which is required to have energy larger than 110 MeV.

Our analysis is based on the "zero-tag" mode, where by collecting small total transverse momentum events, $|\sum \vec{p}_t| < 0.05$ GeV/c, the incident photons are guaranteed to have small virtuality. Under this condition, beam e^+e^- particles are supposed to escape through the beam pipes with small scattering angle and hence the photon-photon collision axis is approximated with the e^+e^- beam axis.

Received 26 January 2010

1) E-mail: nkzw@post.kek.jp

We estimate the fraction of background events by comparing the $|\sum\vec{p}_{\rm t}|$ distribution between data and signal Monte Carlo (MC) events, and subtract them from data in each ΔW-$\Delta|\cos\theta^*|$ bin.

4 Light scalar resonance study

We perform fits to the differential cross section in the W regions of 0.8 GeV $< W <$ 1.6 GeV [8] and 1.7 GeV $< W <$ 2.5 GeV [9] for $\gamma\gamma \to \pi^0\pi^0$, and 0.9 GeV $< W <$ 1.46 GeV for $\gamma\gamma \to \eta\pi^0$ [10], and the angular region of $|\cos\theta^*| < 0.8$, using

$$\frac{{\rm d}\sigma}{4\pi{\rm d}|\cos\theta^*|} = |SY_0^0 + D_0Y_2^0 + G_0Y_4^0|^2 + |D_2Y_2^2 + G_2Y_4^2|^2 = \hat{S}^2|Y_0^0|^2 + \hat{D}_0^2|Y_2^0|^2 + \hat{D}_2^2|Y_2^2|^2 + \hat{G}_0^2|Y_4^0|^2 + \hat{G}_2^2|Y_4^2|^2, \quad (2)$$

where D_0 and G_0 (D_2 and G_2) denote the helicity 0 (2) components of the D and G waves, respectively, and Y_J^m's are the spherical harmonics. Each wave consists of resonance term, e.g.,

$$A_{\rm R}^J(W) = \sqrt{\frac{8\pi(2J+1)m_{\rm R}}{W}}\frac{\sqrt{\Gamma_{\rm tot}\Gamma_{\gamma\gamma}(R)\mathcal{B}(R\to h\bar{h}')}}{m_{\rm R}^2 - W^2 - {\rm i}m_{\rm R}\Gamma_{\rm tot}}, \quad (3)$$

where $\Gamma_{\gamma\gamma}(R)$ and J are the two-photon decay width and spin for the resonance R, respectively, and the coherent background term assumed to be quadratic in W.

4.1 $\gamma\gamma \to \pi^0\pi^0$

The differential cross section is calculated using Eq. (1) with the efficiency estimated from a signal MC study.

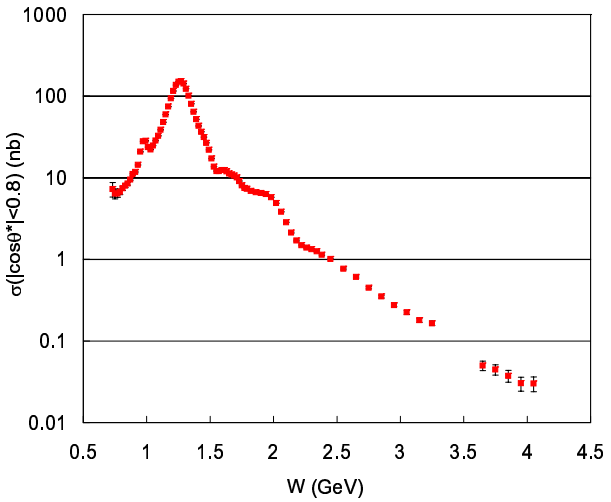

Fig. 1. The total cross section for $\gamma\gamma \to \pi^0\pi^0$ ($|\cos\theta^*| < 0.8$). Data points near in bins near 3.5 GeV are not shown because of uncertainty from the $\chi_{\rm cJ}$ subtraction.

Figure 1 shows the total cross section integrated over $|\cos\theta^*| < 0.8$. We observe clear peaks for the $f_0(980)$ near 0.98 GeV and the $f_2(1270)$ near 1.25 GeV and find at least two more structures around 1.65 and 1.95 GeV.

In the fit to the lower energy region 0.8 GeV $< W <$ 1.6 GeV where S, D_0 and D_2 waves are considered, in addition to $f_0(980)$, $f_2(1270)$ and $f_2'(1575)$ we introduce a scalar meson $f_0(Y)$ to take into account a resonance-like structure around 1.2 GeV seen in $\hat{S}^2$ in Fig. 2, which can be either the $f_0(1370)$ or $f_0(1500)$ or a mixture of them.

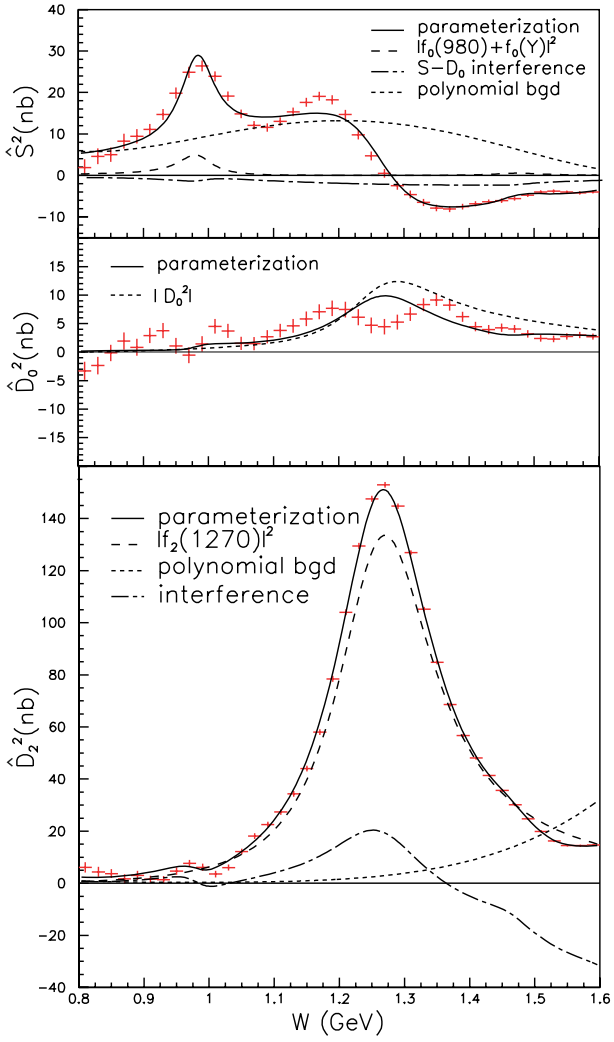

Fig. 2. The $\hat{S}^2$ (top), $\hat{D}_0^2$ (middle), and $\hat{D}_2^2$ (bottom) spectra for $\gamma\gamma \to \pi^0\pi^0$. Curves are results of the fit.

We obtain the fraction of the $f_2(1270)$ component in the D_0 wave, $r_{02} = (3.7 \pm 0.3^{+15.9}_{-0.29})\%$ and $\mathcal{B}(f_2(1270) \to \gamma\gamma) = (1.57 \pm 0.01^{+1.39}_{-0.14}) \times 10^{-5}$. Inclusion of both non-zero value of r_{02} and $f_0(Y)$ is favored over absense of r_{02} and/or $f_0(Y)$. Other fit results are summarized in Table 1.

In the fit to 1.7 GeV $< W <$ 2.5 GeV where the G wave contributions are nonzero and are dominated by the G_2 wave, we assume $f_4(2050)$ in the G_2 wave with its paremeters floated. Since the G_2 wave interferes with the D_2 wave, we include the resonance $f_2(1950)$, which is known to couple to two photons. Here we denote it as the "$f_2(1950)$" assuming that the $f_2(1950)$ is just an empirical parameterization representing any possible resonances in this W region [17]. For $|\cos\theta^*|<0.7$, the $|Y_4^0|^2$ and $|Y_4^2|^2$ terms are nearly equal, so we show $\hat{G}_0^2+\hat{G}_2^2$ and $\hat{G}_0^2-\hat{G}_2^2$ instead.

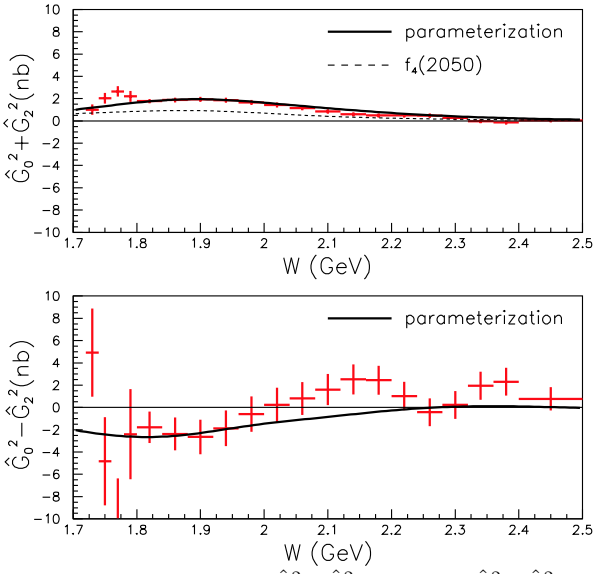

Fig. 3. Spectrum of $\hat{G}_0^2+\hat{G}_2^2$ (top) and $\hat{G}_0^2-\hat{G}_2^2$ (bottom) and fitted curves for $\gamma\gamma\to\pi^0\pi^0$.

The resulting spectra are shown in Figs. 3 and 4, and obtained parameters are listed in Table 1. The $M(f_4(2050))$ and "$M(f_2(1950))$" flip and the widths are about two times larger than their PDG values. Further fit studies reveal that the fits with $f_4(2050)$ parameteres fixed or without "$f_2(1950)$" are disfavored compared to the nominal fit, and a more reasonable fit is obtained when two more parameters are introduced in the G_2 background. Although a more sophisticated model is necessary, our data clearly require a G-wave component, and the unacceptably worse fit without the $f_4(2050)$ strongly supports its finite two-photon coupling.

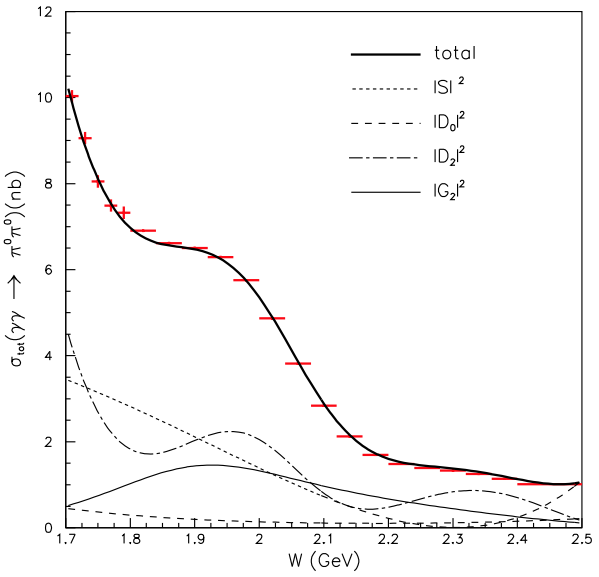

Fig. 4. Cross section ($|\cos\theta^*|<0.8$)(nb) and the fit result curves for $\gamma\gamma\to\pi^0\pi^0$.

Table 1. Fit results for the light scalar mesons.

$\pi^0\pi^0$ (95/fb [8])		$\pi^0\pi^0$ (223/fb [9])		$\eta\pi^0$ (223/fb [10])		unit
Mass($f_0(980)$)	982.2 ± 1.0	Mass($f_4(2050)$)	1885^{+14}_{-13}	Mass($a_0(980)$)	$982.3^{+0.6+3.1}_{-0.7-4.7}$	MeV/c^2
$\Gamma(f_0(980))$	$285.5^{+17.2}_{-17.1}$	$\Gamma(f_4(2050))$	453 ± 20	$\Gamma(a_0(980))$	$75.6\pm1.6^{+17.4}_{-10.0}$	MeV
		$\Gamma_{\gamma\gamma}(\pi^0\pi^0)(f_4(2050))$	$7.7^{+1.2}_{-1.1}$	$\Gamma_{\gamma\gamma}(\eta\pi^0)(a_0(980))$	123^{+3+501}_{-2-43}	eV
Mass(f_0(Y))	1469.7 ± 4.7	Mass("$f_2(1950)$")	2038^{+13}_{-11}	Mass(a_0(Y))	$1316.8^{+0.7+24.7}_{-1.0-4.6}$	MeV/c^2
$\Gamma(f_0$(Y))	$89.7^{+8.1}_{-6.6}$	Γ("$f_2(1950)$")	441^{+27}_{-25}	$\Gamma(a_0$(Y))	$65.0^{+2.1+99.1}_{-5.4-32.6}$	MeV
$\Gamma_{\gamma\gamma}\mathcal{B}(\pi^0\pi^0)$	$11.2^{+5.0}_{-4.0}$	$\Gamma_{\gamma\gamma}\mathcal{B}(\pi^0\pi^0)$	54^{+23}_{-14}	$\Gamma_{\gamma\gamma}\mathcal{B}(\eta\pi^0)$	$432\pm6^{+1073}_{-256}$	eV

4.2 $\gamma\gamma\to\eta\pi^0$

Figure 5 shows the cross section integrated over $|\cos\theta^*|<0.8$ on logarithmic and linear scales for partial W regions. The data points are in good agreement with those from Crystal Ball [13]. We find three resonant structures: near 0.98 GeV ($a_0(980)$), 1.32 GeV ($a_2(1320)$) and 1.7 GeV (probably the $a_2(1700)$). We focus on the region, $W <$ 1.5 GeV, where $J>2$ waves can be safely neglected, because a fit with $a_2(1320)$ parameters doesn't give a stable result. Introducing a_0(Y) to model the shoulder around 1.2 GeV in the $\hat{S}^2$ wave, we fit differential cross sections for the range 0.90 GeV $< W <$ 1.46 GeV (Table 1).

In case the $a_2(1320)$ parameters are floated, we obtain $\mathcal{B}(a_2(1320)\to\gamma\gamma)=(9.4)^{+6.3}_{-2.2}\times10^{-6}$.

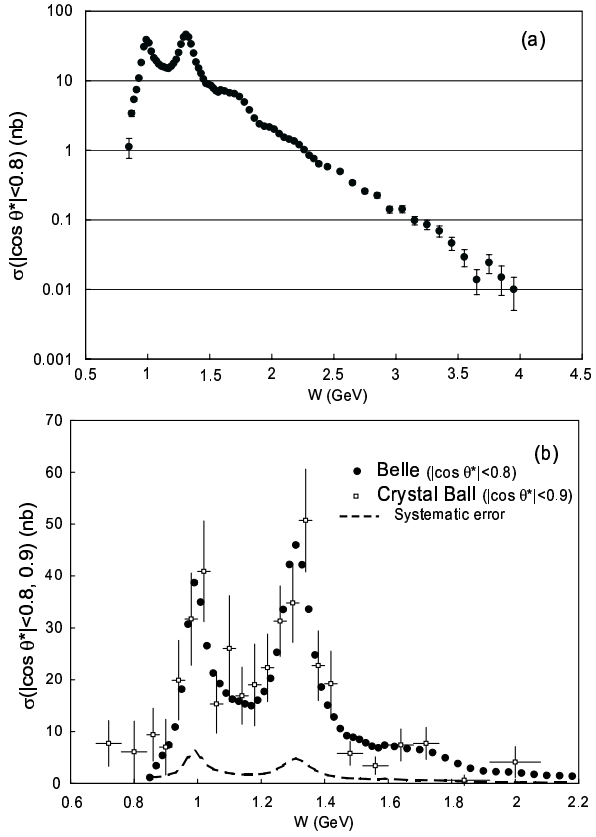

Fig. 5. Cross section for $\gamma\gamma \to \eta\pi^0$ ($|\cos\theta^*| < 0.8$) on (a) logarithmic and (b) linear scale compared with the Crystal Ball measurement ($|\cos\theta^*| < 0.9$) [13]. The corrections for different $|\cos\theta^*|$ coverage are not made. The dashed curve shows the size of the systematic error.

5 Analysis of the higher-energy region

The leading-order QCD calculation [14, 15] predicts $d\sigma(\pi^0\pi^0)/d\sigma(\pi^+\pi^-) \approx 0.07$ at $|\cos\theta^*| = 0$, changing to ≈ 0.4 at $|\cos\theta^*| = 0.6$, and $d\sigma(\eta\pi^0)/d\sigma(\pi^0\pi^0) = 0.46(f_\eta/f_{\pi^0})^2$ where $f_\eta(f_{\pi^0})$ is the $\eta(\pi^0)$ form factor, while $d\sigma(\pi^0\pi^0)/d\sigma(\pi^+\pi^-) = 0.05$ by the handbag model [16]. We can evaluate these predictions at $W > 2.4$ GeV where the contribution from resonances is small.

5.1 $\gamma\gamma \to \pi^0\pi^0$

The normalized differential cross section for selected four W points is shown in Fig. 6(a) where the fit function

$$d\sigma/d|\cos\theta^*| = a(\sin^{-4}\theta^* + b\cos^2\theta^*) \qquad (4)$$

is used. Above $W = 3.1$ GeV, the $\sin^{-4}\theta^*$ dependence ($b = 0$) is also acceptable. The W dependence of b is shown in Fig. 6(b). The cross sections $\sigma(\pi^0\pi^0)$ and $\sigma(\pi^+\pi^-)$, and their ratio which is found to be $0.32 \pm 0.03 \pm 0.05$ for 3.1 GeV $< W <$ 4.1 GeV, are shown in Fig. 7. The power-law W^{-n} dependence parameter of the total cross section ($|\cos\theta^*| < 0.8$) is obtained to be $n = 8.0 \pm 0.5 \pm 0.4$.

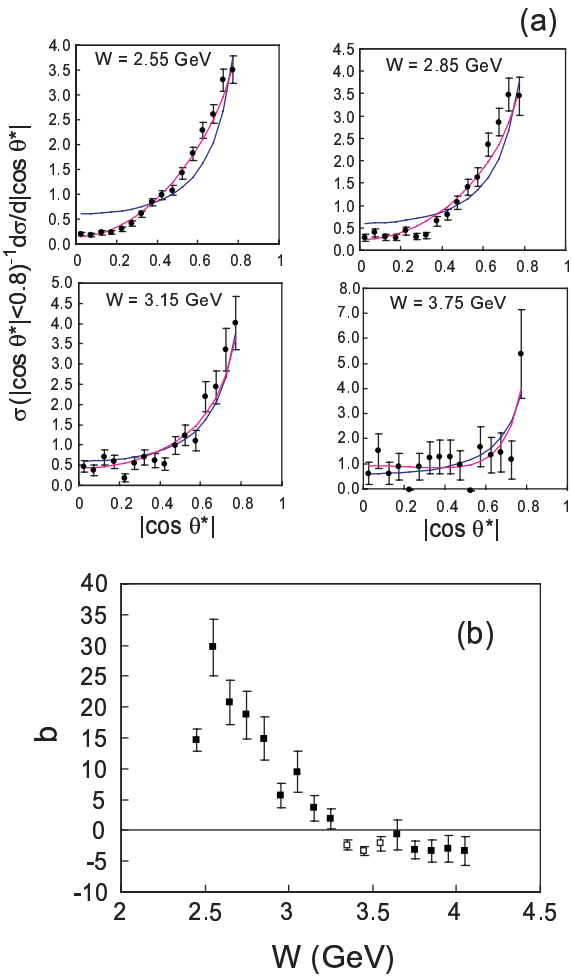

Fig. 6. (a) $\sin^{-4}\theta^*$ fits of the angular dependence with (solid curve) and without (dashed curve) $\cos^2\theta^*$ term. (b) W dependence of b for $\gamma\gamma \to \pi^0\pi^0$. Open squares show the χ_{cJ} meson regions.

5.2 $\gamma\gamma \to \eta\pi^0$

The angular dependence is in agreement with $\sin^{-4}\theta^*$ for $W > 2.7$ GeV. The fit with W^{-n} gives $n = 10.5 \pm 1.2 \pm 0.5$. The n values are summarized in Table 2. The ratio $d\sigma(\eta\pi^0)/d\sigma(\pi^0\pi^0)$ is consistent with leading-order calculation of 0.46 if f_η/f_{π^0} is 1.

6 Conclusion

We have measured the diffential cross sections of the two-photon production of pure neutral final states, $\gamma\gamma \to \pi^0\pi^0$ and $\eta\pi^0$, using a high-statistics

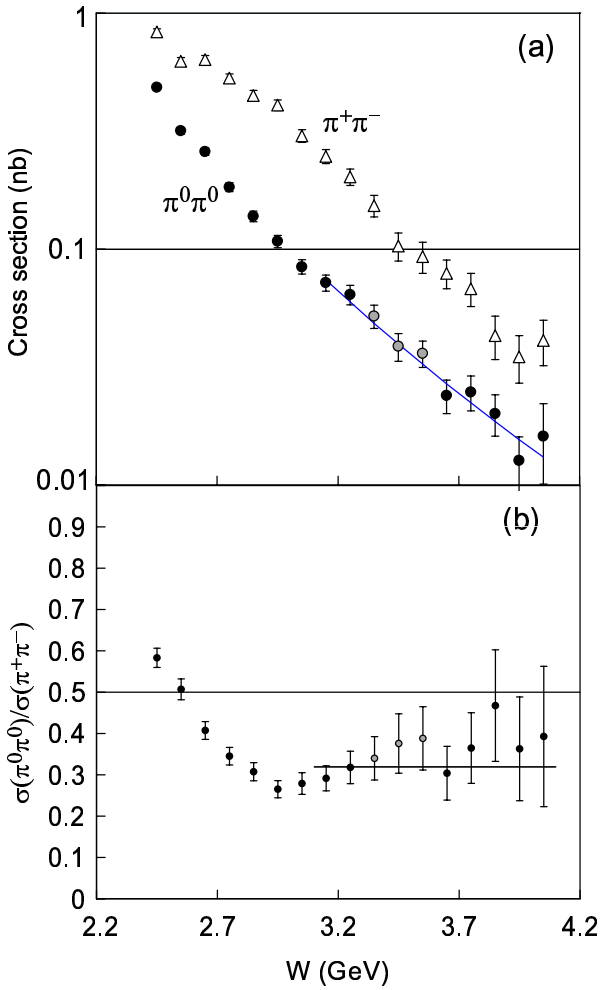

Fig. 7. (a) Cross section for $\gamma\gamma \to \pi^0\pi^0$ (solid circles) with the W^{-n}-dependence fit result, in comparison with and $\pi^+\pi^-$ (triangles) in $|\cos\theta^*| < 0.6$, and (b) their ratio with the constant fit function. χ_{cJ} regions (gray circles) are not used.

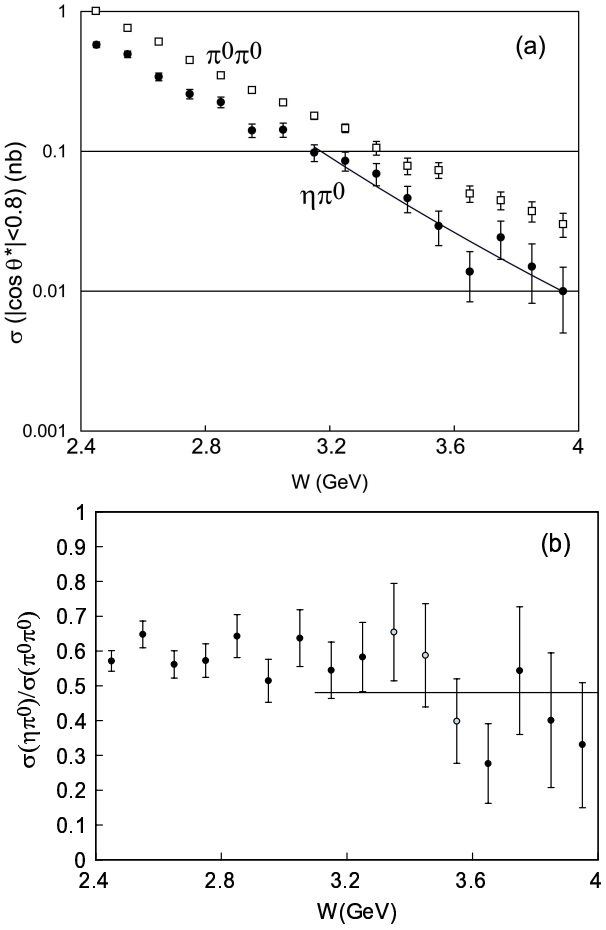

Fig. 8. (a) Cross section for $|\cos\theta^*| < 0.8$ and the power-law fit with (solid curve). (b) The ratio $d\sigma(\eta\pi^0)/d\sigma(\pi^0\pi^0)$. The line shows the average over 3.1–4.0 GeV where the data in the χ_{cJ} regions (gray circles) are not used.

Table 2. Power-low dependence parameters of the cross sections $\sigma \propto W^{-n}$ in various reactions.

process	n	W range/GeV	$\lvert\cos\theta^*\rvert$ range	Ref.
$\eta\pi^0$	$10.5\pm1.2\pm0.5$	3.1–4.1	<0.8	[10]
$\pi^0\pi^0$	$8.0\pm0.5\pm0.4$	3.1–4.1	<0.8	[9]
$\pi^0\pi^0$	$6.9\pm0.6\pm0.7$	3.1–4.1	<0.6	[9]
$\pi^+\pi^-$	$7.9\pm0.4\pm1.5$	3.0–4.1	<0.6	[1]
K^+K^-	$7.3\pm0.3\pm1.5$	3.0–4.1	<0.6	[1]
$K^0_SK^0_S$	$10.5\pm0.6\pm0.5$	2.4–4.0	<0.6	[5]

data sample collected with the Belle detector at the KEKB accelerator. We perform the partial wave analyses in the lower energy region to extract properties of the light scalar mesons.

For 0.8 GeV $< W(\pi^0\pi^0) <$ 1.6 GeV a model including S, D_0 and D_2 waves is tested. The $f_0(Y)$ is necessary in the S wave in addition to the known $f_0(980)$, $f_2(1320)$ and $f'(1525)$ mesons. Our data favor inclusion of $f_0(Y)$ and $f_2(1270)$ contribution to the D_0 wave. For 1.7 GeV $< W(\pi^0\pi^0) <$ 2.5 GeV, a contribution of the $f_4(2050)$ is significant in the G wave. We introduce $a_0(Y)$ to model $d\sigma/d|\cos\theta^*|$ for 0.9 GeV $< W(\eta\pi^0) <$ 1.46 GeV in the fit using S, D_0 and D_2 waves.

In the higher energy region, QCD predictions are compared to the data. The $\sin^{-4}\theta^*$ dependence of the differential cross section is in agreement with the observed data above $W = 3.1(2.7)$ GeV for $\gamma\gamma \to \pi^0\pi^0(\eta\pi^0)$ but an additional $\cos^2\theta$ term gives a better fit to the $\pi^0\pi^0$ data in the 2.4–4.1 GeV region. The power-law dependence of the total cross section, $\sigma \propto W^{-n}$ and their ratios are presented.

References

1 Nakazawa H et al (Belle collaboration). Phys. Lett. B, 2005, **615**: 39
2 Mori T et al (Belle collaboration). Phys. Rev. D, 2007, **75**: 051101(R)
3 Mori T et al (Belle collaboration). J. Phys. Soc. Jpn, 2007, **76**: 074102
4 Abe K et al (Belle collaboration). Eur. Phys. J. C, 2004, **32**: 323
5 CHEN W T et al (Belle collaboration). Phys. Lett. B, 2007, **651**: 15
6 KUO C C et al (Belle collaboration). Phys. Lett. B, 2005, **621**: 41
7 Uehara S et al (Belle collaboration). Phys. Rev. Lett., 2006, **96**: 082003
8 Uehara S et al (Belle collaboration). Phys. Rev. D, 2008, **78**: 052004
9 Uehara S et al (Belle collaboration). Phys. Rev. D, 2009, **79**: 052009
10 Uehara S et al (Belle collaboration). Phys. Rev. D, 2009, **80**: 032001
11 Abashian A et al (Belle collaboration). Nucl. Instr. and Meth. A, 2002, **479**: 117
12 Kurokawa S, Kikutani E. Nucl. Instr. and Meth. A, 2003, **499**: 1, and other papers included in this Volume
13 Antreasyan D et al (Crystal Ball collaboration). Phys. Rev. D, 1986, **33**: 1847
14 Brodsky S J, Lepage G P. Phys. Rev. D, 1981, **24**: 1808
15 Benayoun M, Chernyak V L. Nucl. Phys. B, 1990, **329**: 285
16 Diehl M, Kroll P, Vogt C. Phys. Lett. B, 2002, **532**: 99
17 YAO W M et al (Particle Data Group). J. Phys. G, 2006, **33**: 1